2005 International Nuclear Atlantic Conference - INAC 2005
Santos, SP, Brazil, August 28 to September 2, 2005

OPTIMIZATION PROCEDURE TO DESIGN PRESSURIZER EXPERIMENTS

David A. Botelho, Paulo A. B. De Sampaio, Celso M. F. Lapa, Cláudio M. N. A. Pereira, and Maria de Lourdes Moreira, ***Instituto de Engenharia Nuclear, Rio de Janeiro***

Antônio Carlos de O. Barroso, ***IPEN, São Paulo***

ABSTRACT

The proper choice of the pressure number was employed to obtain the best form of the non-dimensional conservation equations for a two-volume pressurizer. This form and the non-dimensional constitutive models, define the similarity numbers of scaled systems similar to the IRIS reactor pressurizer. The similarity numbers represent the scaled transport of mass and energy, and of the local rainout, flashing, and wall condensation mass and energy transport. The genetic algorithm (GA) search variables of scaled models are the geometric sizes, the surge mass flow rate, and the heater power needed to control the pressure. The similarity numbers are used to define a "fitness function" to evaluate the quality of the defined variables. The operation of the systems is verified using a two-volume transient model to simulate a typical out-surge transient. The agreement of the non-dimensional pressure as the model pressure increases, and the good agreement of the non-dimensional volumes of different scaled systems recommends this non-dimensional formalism, the GA optimization, and the numeric simulation of a surge transient, to design scaled experiments for modeling the IRIS pressurizer.

1. INTRODUCTION

The IRIS reactor pressurizer is contained within the integral vessel upper head that is the upper boundary of the vapor volume. Because of its large volume, the IRIS pressurizer does not need a spray system of sub-cooled liquid to reduce pressure increments due to in-surge transients, but heaters are provided in the liquid volume of the pressurizer to control the out-surge transients. The liquid volume is separated from the circulating reactor coolant by a steel structure through it surge liquid flows. The pressurizer layout is shown in Figure 1.

2. THE MASS AND ENERGY CONSERVATION

The upper vapor volume may contain liquid drops, and vapor bubbles may be generated in the lower liquid volume. The two-volume model of the pressurizer comprises the upper volume of vapor and the lower volume of liquid assuming that the liquid drops and the liquid condensed on the walls fall into the liquid volume, while the vapor bubbles rise to the vapor volume [1]. The volume averaged mass and energy conservation equations, the constitutive models, and the state equations represent the transient vapor and the liquid mass and energy. The non-dimensional mass and energy balance equations in the two-volume pressurizer are:

$$\frac{d}{dt'}\left(m_v'\right) = W_{FL}' - W_{RO}' - W_{WC}' \tag{1}$$

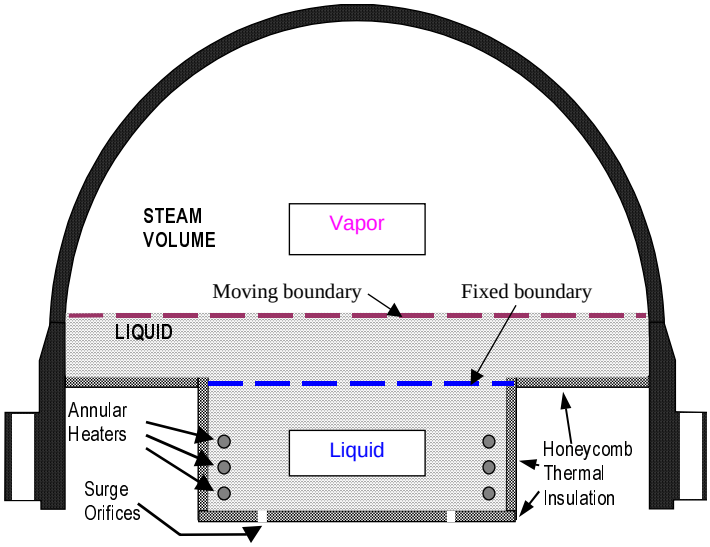

Figure 1. The IRIS pressurizer layout

$$\frac{d}{dt'}\left(m_l'\right) = -W_{FL}' + W_{RO}' + W_{WC}' + \dot{m}_{surge}' \tag{2}$$

$$\frac{d}{dt'}\left(m_v' h_v'\right) = \left(W_{FL}' - W_{WC}'\right) h_g' - W_{RO}' h_f' + \left(\frac{p^0 v_{fg}^0}{h_{fg}^0}\right) m_v' v_v' \frac{dp'}{dt'} \tag{3}$$

$$\begin{aligned}\frac{d}{dt'}\left(m_l' h_l'\right) = {} & \left(W_{RO}' + W_{WC}'\right) h_f' - W_{FL}' h_g' + \left(\frac{p^0 v_{fg}^0}{h_{fg}^0}\right) m_l' v_l' \frac{dp'}{dt'} \\ & + \dot{m}_{surge}' h_{surge}' + \left(\frac{\dot{Q}_h^0}{\dot{m}_{surge}^0 h_{fg}^0}\right) \dot{Q}_{heater}'\end{aligned} \tag{4}$$

The primed variables in the Eqs. (1)-(4) are non-dimensional. The 0 superscript parameters are reference values. The m_v', m_l', h_v', and h_l' are the non-dimensional unknowns in these equations. The W_{FL}', W_{RO}', and W_{WC}' are non-dimensional mass flow rates which are obtained through specific non-dimensional constitutive equations. The constitutive equations, in turn, introduce new non-dimensional numbers, as defined later in this report. All other prime variables are non-dimensional that need to be made equal in a similar model. The similarity concept is defined later in this report. The surge mass flow rate prime variable is a given function that is equal in all scales. For in-surge, the surge enthalpy, h_{surge}', is a given function, that is the same in all scales. For out-surge, the surge enthalpy prime variable is a function of the solution, hence $h_{surge}' = h_l / h_{fg}^0$.

The reference time used in the Eqs. (1)-(4) is the reference mass divided by the reference mass flow rate. Due to this reference time, the mass equations introduce only the non-dimensional mass flow rates that, as mentioned, may introduce non-dimensional numbers through respective constitutive equations.

The prime variables, h'_f and h'_g, in Eqs. (3) and (4) are expanded in the neighborhood of the reference pressure, respectively, as

$$h'_f = \frac{h_f}{h^0_{fg}} = \frac{h^0_f}{h^0_{fg}} + \frac{p_0}{h^0_{fg}}\left(\frac{d\,h_f}{d\,p}\right)_0 (p' - 1) \tag{5}$$

$$h'_g = \frac{h_g}{h^0_{fg}} = \frac{h^0_g}{h^0_{fg}} + \frac{p_0}{h^0_{fg}}\left(\frac{d\,h_g}{d\,p}\right)_0 (p' - 1) \tag{6}$$

Besides these non-dimensional, in the energy equations appear two additional non-dimensional factors: the pressure number and the heat source power number, which are, respectively, defined as

$$\left(NP^0_{pres}\right) = \frac{p^0 v^0_{fg}}{h^0_{fg}} = \Psi^0 \tag{7}$$

$$\left(N\dot{Q}^0_{heater}\right) = \frac{\dot{Q}^0_h}{\dot{m}^0_{surge} h^0_{fg}} \tag{8}$$

3. THE LOCAL PHENOMENA

The closure equations in non-dimensional form represent the scaled mechanisms of rainout, flashing, and wall condensation. The model derived by Nusselt [2] defines the heat rate of wall condensation as

$$\dot{Q}_{WC} = \frac{4k_f}{3L_v}\left(\frac{g\,\rho_f\left(\rho_f - \rho_g\right)h_{fg}\left(L_v\right)^3}{4\mu_f\,k_f\left(T_v - T_w\right)}\right)^{1/4} S_v\left(T_v - T_w\right) \tag{9}$$

The non-dimensional form of Eq. (9) is

$$\dot{Q}'_{WC} = \left(N\dot{Q}^0_{WC}\right) h'_{WC}\, S'_v \left(T'_v - T'_w\right) \tag{10}$$

where the wall condensation heat number is defined as

$$\left(N\dot{Q}^0_{WC}\right)=\frac{4}{3}\left(\frac{g\left(\rho^0\right)^2 h^0\left(L^0\right)^3}{4\mu^0\ k^0\ T^0}\right)^{1/4}\times\left(\frac{A^0 k^0 T^0/L^0}{\dot{Q}^0_h}\right) \tag{11}$$

The mass flow rate associated to wall condensation is

$$W_{WC}=\frac{\dot{Q}_{WC}}{h_{fg}} \tag{12}$$

The non-dimensional form of the wall condensation Eq. (12) is

$$W'_{WC}=\frac{\dot{Q}^0_h\dot{Q}'_{WC}}{\dot{m}^0_{surge}h^0_{fg}h'_{fg}}=\left(N\dot{Q}^0_{heater}\right)\left(N\dot{Q}^0_{WC}\right)\frac{h'_{WC}S'_v\left(T'_v-T'_w\right)}{h'_{fg}} \tag{13}$$

Eq. (13) defines a mass flow wall condensation number as

$$\left(NW^0_{WC}\right)=\left(N\dot{Q}^0_{heater}\right)\left(N\dot{Q}^0_{WC}\right) \tag{14}$$

Liquid drops are generated in the vapor volume due to bulk condensation (rainout) and flow through the liquid interface. The drag force is neglected because the acceleration resulting from the drop weight and the buoyancy reaction force is small in the equation of motion of a single liquid drop. The non-dimensional equation of motion of a liquid drop is

$$\frac{d^2y'}{dt'^2}=\left(\frac{gL_0}{u_0^2}\right)\times\left(\frac{\rho'_f-\rho'_g}{\rho'_f}\right) \tag{15}$$

The similarity number for the local phenomena of rainout is defined as the inverse of the Froude number. The rainout number and the Froude number are defined as

$$\left(NW^0_{RO}\right)=\frac{1}{Fr}=\frac{gL^0}{u_0^2} \tag{16}$$

The rainout mass flow rate is

$$W_{RO}=\rho_f\ u_d\left(1-\alpha_v\right)A_{lv} \tag{17}$$

where the velocity that the liquid drop reaches the liquid interface is

$$u_d = \sqrt{gL_v\left(\frac{v_v - v_f}{v_v}\right)} \tag{18}$$

The non-dimensional form of the rainout mass flow rate Eq. (17) is

$$W'_{RO} = \frac{\rho'_f\ \rho^0\ u'_d\ u^0(1-\alpha_v)A^0A'_{lv}}{\dot{m}^0_{surge}} = (1-\alpha_v)\rho'_f\ u'_d\ A'_{lv} \tag{19}$$

Vapor bubbles are generated in the liquid volume due to bulk evaporation (flashing) and flow through the liquid interface into the vapor volume. Because the acceleration resulting from the bubble weight and the buoyancy reaction force is large, it is necessary to include the drag force in the equation of motion of a vapor bubble in the liquid volume. If the bubble terminal velocity is calculated using the Zuber formula [3],

$$u_b = 1.41\left[\frac{\sigma\ g\ (\rho_f - \rho_g)}{\rho_f^2}\right]^{1/4} \tag{20}$$

the non-dimensional equation of motion of a vapor bubble is

$$\begin{aligned}\frac{d^2y'}{dt'^2} &= \left(\frac{\Delta\rho}{\rho_g}\right)^0 \frac{gL_0}{u_0^2}\left(\frac{\rho'_f - \rho'_g}{\rho'_g}\right) \\ &- \left[\left(\frac{\Delta\rho}{\rho_g}\right)^0 \frac{g\rho^0(L^0)^2}{\sigma^0}\right]^{1/2} \frac{1}{2}\left[\frac{\rho'_f - \rho'_g}{\rho'_g}\left(\frac{\rho'_f}{\rho'_g}\right)\frac{\rho'_f}{\sigma'}\right]^{1/2}\left(\frac{dy'}{dt'}\right)^2\end{aligned} \tag{21}$$

The reference difference density ratio is fixed for a given pressure. The Froude number, Fr, equivalence is necessary for the rainout similarity. The flashing number is obtained from the ratio of square of the non-dimensional factor that appears in the drag force, to the non-dimensional factor in the gravitational force term of Eq. (21). The flashing number is thus defined as

$$(NW^{\ 0}_{FL}) = \left(\frac{\Delta\rho}{\rho_g}\right)^0 \rho_f^{\ 0}\ \frac{L^0\ u_0^{\ 2}}{\sigma^{\ 0}} \tag{22}$$

If the bubble terminal velocity is calculated using the Wilson formula [4],

$$u_b = \gamma_l \left[g \left(\frac{\sigma}{g\left(\rho_f - \rho_g\right)} \right)^{0.5} \right]^{0.5} \tag{23}$$

the non-dimensional equation of motion of a vapor bubble is

$$\begin{aligned} \frac{d^2 y'}{d t'^2} = & \left(\frac{\Delta\rho}{\rho_g} \right)^0 \frac{g L_0}{u_0^2} \left(\frac{\rho'_f - \rho'_g}{\rho'_g} \right) \\ & - \frac{1}{\gamma_l^2} \left(\frac{\Delta\rho}{\rho_g} \right)^0 \left(\frac{\rho'_f - \rho'_g}{\rho'_g} \right) \left(\rho_f^0 \frac{g L_0^2}{\sigma^0} \right)^{0.5} \left(\frac{\rho'_f - \rho'_g}{\sigma'} \right)^{0.5} \left(\frac{d y'}{d t'} \right)^2 \end{aligned} \tag{24}$$

The bubble non-dimensional velocity, γ_l, is assumed, in the model pressurizer, of the same magnitude of that in the IRIS pressurizer. Therefore, the same Eq. (22) expression for the flashing number is obtained. In the second derivation, the flashing number is also defined as the ratio of square of the non-dimensional factor that appear in the drag force, to the non-dimensional factor in the gravitational force term of Eq. (24).

The flashing mass flow rate is

$$W_{FL} = \rho_g \, u_b \, \alpha_l \, A_{lv} \tag{25}$$

The non-dimensional form of the flashing mass flow rate Eq. (25) is

$$W'_{FL} = \frac{\rho'_g \, \rho^0 \, u'_b \, u^0 \, \alpha_l \, A^0 A'_{lv}}{\dot{m}^0_{surge}} = \alpha_l \, \rho'_g \, u'_b \, A'_{lv} \tag{26}$$

The substitution of Eqs. (5) and (6) into the equations (3) and (4) introduce eight new non-dimensional numbers. As the rain-out mass flow equation Eq. (19) and the flashing mass flow equation Eq. (26) do not introduce new non-dimensional numbers, the similarity numbers associated with the enthalpy transport by rain-out and flashing are defined, respectively, as

$$\left(NWh^0_{RO}\right)_1 = \frac{h^0_f}{h^0_{fg}} \tag{27}$$

$$\left(NWh^0_{RO}\right)_2 = \frac{p_0}{h^0_{fg}} \left(\frac{d\, h_f}{d\, p} \right)_0 \tag{28}$$

$$\left(NWh_{FL}^{0}\right)_1 = \frac{h_g^0}{h_{fg}^0} \tag{29}$$

$$\left(NWh_{FL}^{0}\right)_2 = \frac{p_0}{h_{fg}^0}\left(\frac{d\,h_g}{d\,p}\right)_0 \tag{30}$$

As the mass flow wall condensation equation Eqs. (13) introduces the mass flow wall condensation number, defined in Eq. (14), the similarity numbers associated with the enthalpy transport by wall condensation are defined as

$$\left(NWh_{WC}^{0}\right)_1 = \left(NW_{WC}^{0}\right)\frac{h_f^0}{h_{fg}^0} \tag{31}$$

$$\left(NWh_{WC}^{0}\right)_2 = \left(NW_{WC}^{0}\right)\frac{h_g^0}{h_{fg}^0} \tag{32}$$

$$\left(NWh_{WC}^{0}\right)_3 = \left(NW_{WC}^{0}\right)\frac{p_0}{h_{fg}^0}\left(\frac{d\,h_f}{d\,p}\right)_0 \tag{33}$$

$$\left(NWh_{WC}^{0}\right)_4 = \left(NW_{WC}^{0}\right)\frac{p_0}{h_{fg}^0}\left(\frac{d\,h_g}{d\,p}\right)_0 \tag{34}$$

4. THE PI CONTROLER

In a transient of out-surge, the pressure can be controlled by a PI controller [5]. The equation for the heater bank control can be put in a non-dimensional form as

$$\dot{Q}'_{heater} = \dot{Q}'_{PI} = K_p\left(1-p'\right) + \frac{m^0 K_i}{\dot{m}^0}\int_{t'_0}^{t'}\left(1-p'\right)dt' \tag{35}$$

As the PI controller is employed to simulate the dynamic behavior of the pressurizer, the substitution of Eq. (35) into Eq. (4) define new similarity numbers. These new similarity numbers are the proportional and integral numbers, defined respectively, as

$$\left(NK_p^0\right) = K_p\left(\frac{\dot{Q}_h^0}{\dot{m}_{surge}^0 h_{fg}^0}\right) \tag{36}$$

$$\left(NK_i^0\right) = \frac{m^0 K_i}{\dot{m}_{surge}^0}\left(\frac{\dot{Q}_h^0}{\dot{m}_{surge}^0 h_{fg}^0}\right) \tag{37}$$

These PI controller numbers of Eqs. (36) and (37) substitute the heat source number.

5. SIMILARITY

In general, similar systems are those represented by the same equations. For similarity, it is sufficient the equality of all the corresponding similarity numbers of the scaled models and the full-scale system. In a scale optimization, the values of the similarity numbers are used to define the parameters of the scaled system. Due to the impossibility to match the prime variables (that are not the unknowns) with different pressure, it can be attained only an approximate similarity. The pressure numbers of the full scale and of the scaled systems with smaller pressure are shown in the in third column of Table 1.

Table 1. Pressure number for the IRIS and the model pressurizer.

Pressure P (MPa)	P x Vf / Hfg	Ψm = P x Vfg / Hfg	ε = (1-Ψm /Ψp)
15.5	0.027366	Ψp = 0.13038	0.00
10.0	0.011016	0.12581	0.03149
5.0	0.003928	0.11636	0.1047
2.5	0.001628	0.10699	0.1794
0.5	0.000259	0.0886	0.3179
0.2	0.000096	0.0803	0.3818

All scaled models with smaller pressure can only be designed with approximate similarity, due to the distortion in the pressure number. The pressure number as defined in Table 1 have "self similarity", which is defined as the repetition of details at descending scales [6]. If the liquid density were defined as reference (column 2), the resulting pressure number would be much more distorted. The last column of Table 1 shows the distortion in the pressure number with reduced pressure.

6. GENETIC ALGORITHM OPTIMIZATION

Genetic algorithms are optimization methods that associate a biologic "chromosome" composed of binary numbers to each search variable [7]. The chromosomes can suffer

mutations and can suffer mitosis. Thus they can split and each half can recombine with another representing the same search variable. The chromosomes set represent the set of the search variables. Each generation set is evaluated through fixed attributes, the best adapted generations has more chance of survival and of passing their genes or characteristics to future generations.

Fixing the pressure of a scaled model, one search variable is the radius of the hemisphere as in the IRIS pressurizer [8]. The other dimensions are in a linear proportion. The remaining search variables are the surge mass flow rate and the heater thermal power. Several sets of these variables are defined and tested by the genetic algorithm (GA). The tests are made using as attribute a "fitness function" (FIT) that contains the square of the differences between respective similarity numbers of the scaled system and the full-scale pressurizer. The fitness function is defined as

$$FIT = \sqrt{\frac{\sum_{i=0}^{14} w_i \left(1 - N_i^m / N_i^P\right)^2}{\sum_{i=0}^{14} w_i}} \tag{38}$$

In Eq. (38) N_i^P represent the similarity numbers of the IRIS pressurizer and N_i^m those of the scaled model, as defined in the Nomenclature, and w_i are weighting numbers. The weighting numbers used were $w_0 = w_1 = \cdots = w_{14} = 1$.

The out-surge test transient in IRIS pressurizer is driven by a mass flow rate curve having a maximum (negative) of -54,84 kg/s [8]. An adequate PI controller can control the transient. The maximum heat power of the proportional bank of the PI controller is 1 MW. This transient requires different sizes for scaled models, as defined by GA. The parameters of the PI controller can also be calculated by GA algorithm, and was done for the consistency test. Nevertheless, it was observed that the GA search always matched the similarity numbers of the controller. Therefore, the parameters of the controller of the models with reduced pressure were calculated from the exact equality of their corresponding similarity numbers.

The consistency of the method is verified searching the parameters of a full pressure system similar to the IRIS pressurizer. In the GA search, the ranges of the search variables are shown in Table 2. The obtained variables are shown in Table 3.

Table 2. Ranges of the pressurizer variables.

Hemispheric radius	Surge mass flow rate	Heating power
0.31115 m to 3.1115 m	5.484 kg to 54.84 kg	10 kW to 1000.0 kW

Table 3. Consistency test data for the IRIS pressurizer.

Pressure (MPa)	Hemispheric radius (m)	Surge mass flow rate (Maximum), (kg/s)	Heating power (Maximum), (kW)
15.5	3.1115	54.84	1000.0
15.5 (*)	3.0239	51.75	937.61

The consistency test in the PI controller numbers of the scaled system of Table 3 is shown in Table 4. The size data of the small-scaled models are shown in Table 5. The similarity numbers for the models are shown in Tables 6, 7, and 8. An asterisk marks the consistency data (*) in these Tables. It is shown that the similar pressurizer in the same pressure reaches excellent agreement in all similarity numbers for a final discrepancy of ~ 0.0138 in the final fitness function. Figure 2 shows the good agreement also obtained for the non-dimensional pressure curve of the outsurge transient for the similar pressurizer with same pressure.

Table 4. PI Controller numbers for the IRIS pressurizer.

Pressure (MPa)	NK_p^0	NK_i^0
15.5	3.4392	9.7672e-9
15.5 (*)	3.4392	9.7672e-9

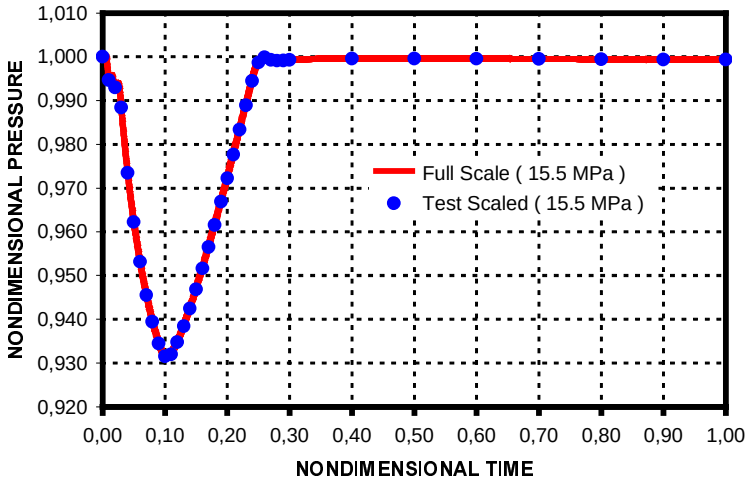

Figure 2. Non-dimensional pressure for the similar pressurizer with same pressure.

The similarity numbers of the controller of all models matches the respective numbers of IRIS pressurizer, presented in Table 4. As expected, the discrepancy in the similarity numbers increase when the pressure decreases. It is shown by the relative deviation in the wall condensation number, that the local phenomena most difficult to attain similarity in a much-reduced pressure are wall condensation. The deviations in the similarity numbers cause the distortion in the solution of the pressurizer Eqs. (1)-(4) for the small-scaled models.

Table 5. Size data for the model pressurizer.

Pressure (MPa)	Hemispheric radius (m)	Surge mass flow rate (Maximum), (kg/s)	Heating power (Maximum), (kW)
10.0	2.6434	51.1719	558.4416
5.0	1.6512	30.0	150.0
2.5	1.2394	20.0	60.0
0.5	1.5237	25.0	25.0
0.2	1.5285	10.0	6.1877

Table 6. Similarity numbers for the IRIS and the model pressurizer (A).

Pressure (MPa)	$\left(NW_{WC}^{0}\right)_0$	$\left(NW_{WC}^{0}\right)_1$	$\left(NW_{WC}^{0}\right)_2$	$\left(NW_{WC}^{0}\right)_3$	$\left(NW_{WC}^{0}\right)_4$
15.5	0.32811	0.55338	0.20831	0.88148	0.15564
15.5 (*)	0.33288	0.56143	0.21134	0.89431	0.15790
10	0.51007	0.54501	0.16668	1.10551	0.06995
5	0.87080	0.61312	0.16537	1.4839	0.021687
2.5	1.2552	0.65621	0.16751	1.9114	0.0008228
0.5	3.2962	1.0011	0.25274	4.2973	0.070473
0.2	10.822	2.4808	0.65541	13.303	0.22770

Figures 3 to 7 show the degree of agreement that can be obtained for the non-dimensional pressure curve of the outsurge transient of the similar pressurizer with reduced pressures. Despite the fact that experiments with much reduced pressure as 0.2 MPa or 0.5 MPa, have much distorted non-dimensional pressure, the variation in the pressure still permit experimental measurement for code validation. A much better experiment, the 2.5 MPa experiment, certainly is adequate and acceptable by the licensing authority for code validation.

Table 7. Similarity numbers for the IRIS and the model pressurizer (B).

Pressure (MPa)	$\left(NW_{RO}^{0}\right)_1$	$\left(NW_{RO}^{0}\right)_2$	$\left(NW_{FL}^{0}\right)_1$	$\left(NW_{FL}^{0}\right)_2$
15.5	1.6866	0.63489	2.6866	0.47436
15.5 (*)	1.6866	0.63489	2.6866	0.47436
10.0	1.0685	0.32678	2.0685	0.13717
5.0	0.70408	0.18991	1.7041	0.024904
2.5	0.52280	0.13346	1.5228	0.006555
0.5	0.30370	0.076675	1.3037	0.021380
0.2	0.22924	0.060564	1.22992	0.021941

Table 8. Similarity numbers for the IRIS and the model pressurizer.

Pressure (MPa)	$N\dot{Q}_{WC}^{0}$	NW_{RO}^{0}	NW_{FL}^{0}	FIT
15.5	17.388	8.5569e5	35.805	
15.5 (*)	17.641	8.3300e5	34.739	0.01381
10.0	27.031	5.8344e5	40.921	0.36950
5.0	46.147	2.0586e5	68.354	0.81692
2.5	66.517	1.2737e5	104.67	1.2915
0.5	174.68	2.7493e5	278.74	3.9064
0.2	573.49	1.8527e6	92.158	12.296

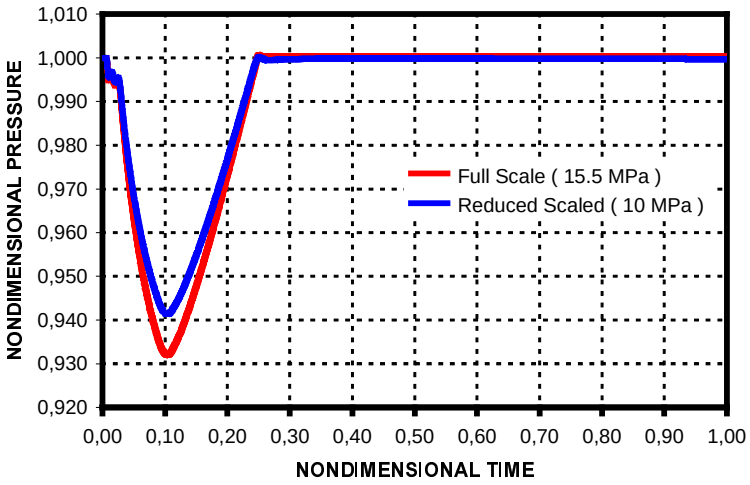

Figure 3. Non-dimensional pressure for IRIS and the model pressurizer (10 MPa).

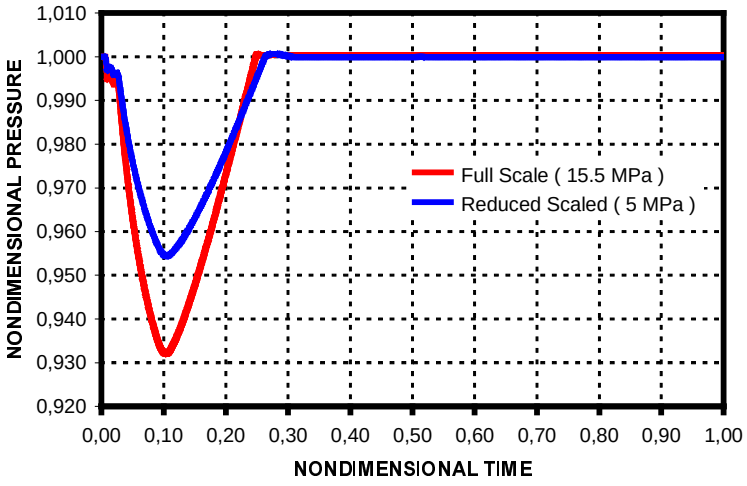

Figure 4. Non-dimensional pressure for IRIS and the model pressurizer (5 MPa).

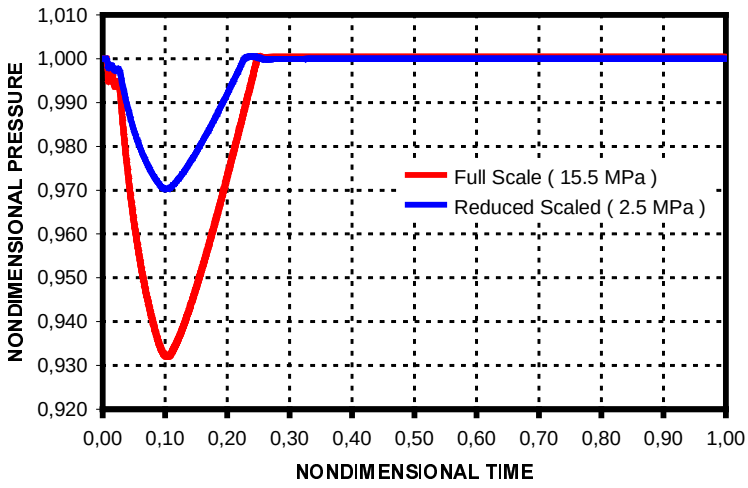

Figure 5. Non-dimensional pressure for IRIS and the model pressurizer (2.5 MPa).

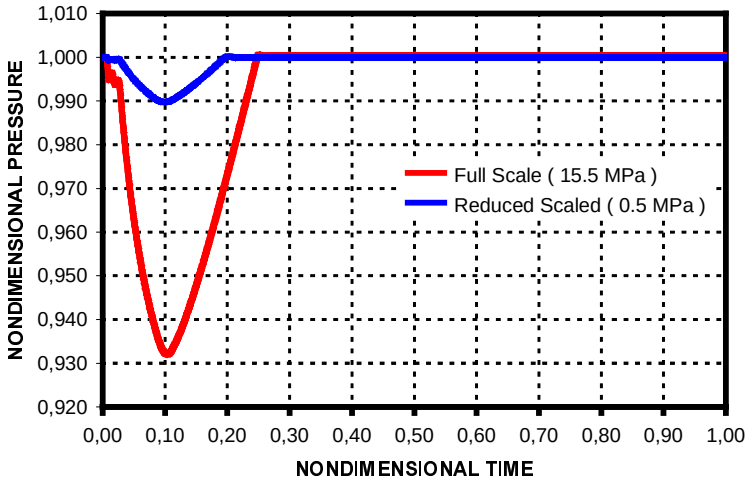

Figure 6. Non-dimensional pressure for IRIS and the model pressurizer (0.5 MPa).

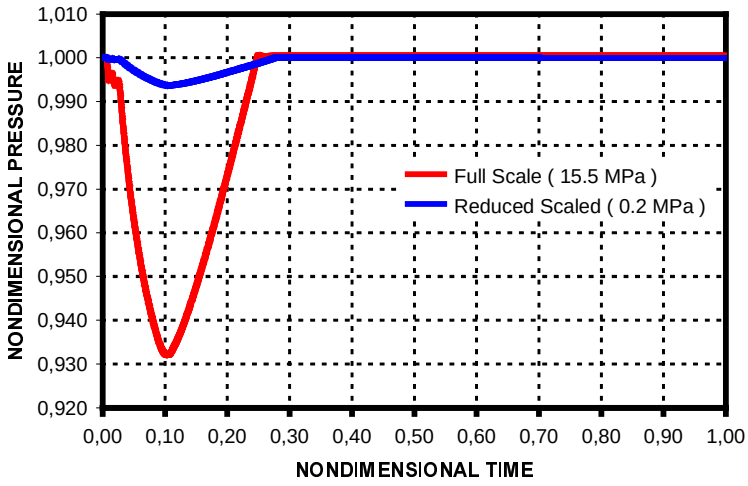

Figure 7. Non-dimensional pressure for IRIS and the model pressurizer (0.2 MPa).

Despite the discrepancy in these numbers, the transient simulations, presented in Figure 3 to Figure 7, show that the non-dimensional pressure curves of the models, tend to the curve of the IRIS pressurizer prototype when the pressure of the models increase. It is observed that the non-dimensional time for the minimum pressure is approximately the same in all scaled models.

Although the largest distorted pressure is for the model with 0.2 MPa, the non-dimensional vapor and liquid volumes still show good agreement with the IRIS transient results, as shown, respectively, in Figures 8 and 9.

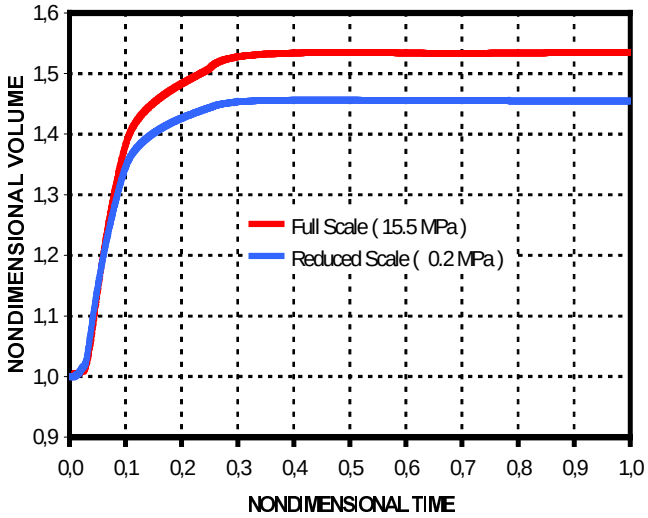

Figure 8. The vapor volume for the IRIS and the model pressurizer.

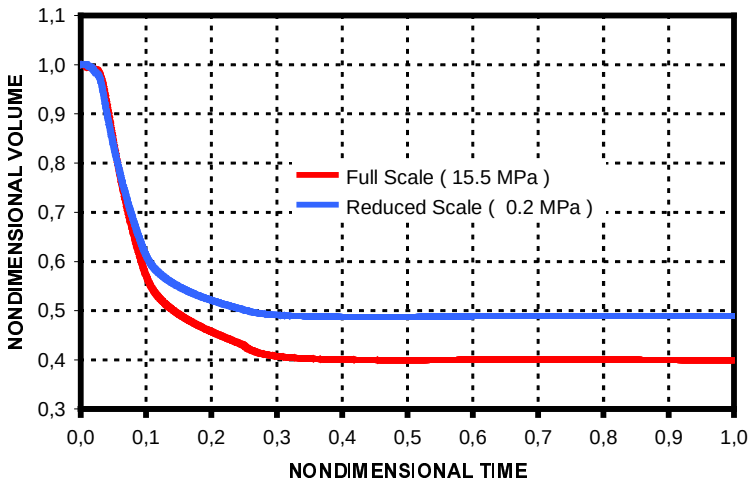

Figure 9. The liquid volume for the IRIS and the model pressurizer.

7. FUTURE WORK

In a future work, new non-dimensional numbers will be incorporated in a new fitness function. These new numbers will substitute the pressure number. To complete the description, the derivation of these numbers is included in this section.

Using the homogeneous model, the specific volume in the vapor volume is calculated as

$$v_v = \left(\frac{h_v - h_f}{h_{fg}} \right) \frac{v_g}{\alpha_v} \tag{39}$$

Therefore, the non-dimensional form of Eq. (39) is

$$v'_v = \left(h'_v - h'_f \right) \frac{v'_g}{\alpha_v} \tag{40}$$

The variable v'_g is expanded in the neighborhood of the reference pressure as

$$v_g' = \frac{v_g}{v_{fg}^0} = \frac{v_g^0}{v_{fg}^0} + \frac{p^0}{v_{fg}^0}\left(\frac{d\,v_g}{d\,p}\right)_0 (p' - 1) \tag{41}$$

The substitution of Eq. (5) and Eq. (41) into Eq. (40) result,

$$v_v' = \left(h_v' - \frac{h_f^0}{h_{fg}^0} - \frac{p_0}{h_{fg}^0}\left(\frac{d\,h_f}{d\,p}\right)_0 (p' - 1)\right)\frac{1}{\alpha_v}\left(\frac{v_g^0}{v_{fg}^0} + \frac{p_0}{v_{fg}^0}\left(\frac{d\,v_g}{d\,p}\right)_0 (p' - 1)\right) \tag{42}$$

The substitution Eq. (42) into Eq. (3) will introduce four additional non-dimensional numbers. They are

$$\Psi_1^0 = \frac{p^0 v_{fg}^0}{h_{fg}^0}\left(\frac{h_f^0}{h_{fg}^0}\right)\left(\frac{v_g^0}{v_{fg}^0}\right) = \frac{p^0}{\left(h_{fg}^0\right)^2} h_f^0 v_g^0 \tag{43}$$

$$\Psi_2^0 = \frac{p^0 v_{fg}^0}{h_{fg}^0}\left(\frac{p^0}{h_{fg}^0}\left(\frac{d\,h_f}{d\,p}\right)_0\right)\left(\frac{v_g^0}{v_{fg}^0}\right) = \left(\frac{p^0}{h_{fg}^0}\right)^2 v_g^0 \left(\frac{d\,h_f}{d\,p}\right)_0 \tag{44}$$

$$\Psi_3^0 = \frac{p^0 v_{fg}^0}{h_{fg}^0}\left(\frac{h_f^0}{h_{fg}^0}\right)\frac{p^0}{v_{fg}^0}\left(\frac{d\,v_g}{d\,p}\right)_0 = \left(\frac{p^0}{h_{fg}^0}\right)^2 h_f^0 \left(\frac{d\,v_g}{d\,p}\right)_0 \tag{45}$$

$$\Psi_4^0 = \frac{p^0 v_{fg}^0}{h_{fg}^0}\frac{p^0}{h_{fg}^0}\left(\frac{d\,h_f}{d\,p}\right)_0 \frac{p^0}{v_{fg}^0}\left(\frac{d\,v_g}{d\,p}\right)_0 = \left(\frac{p^0}{h_{fg}^0}\right)^2 \left(\frac{d\,h_f}{d\,p}\right)_0 p^0 \left(\frac{d\,v_g}{d\,p}\right)_0 \tag{46}$$

When the same procedure is done for the specific volume in the liquid volume, the same numbers will be generated, because it involves, again, the expansion of v_g' and h_f' in the neighborhood of the reference pressure.

8. CONCLUSIONS

Because of the smaller distortion in the pressure number, the form obtained of the non-dimensional mass and energy equations shall always be used. The derivation of non-dimensional constitutive models is of great relevance to scale the local phenomena of rainout, flashing and wall condensation in a scaled model. The GA defined the model parameters

(size, flow rate, power, and the PI control constants). For this definition, the sum of the square of the differences between respective similarity numbers was minimized. This GA optimization is a much valuable tool to obtain the parameters for the model. Without the GA or other good optimization algorithm, the individual designer would have much difficulty to define the best parameters. The agreement of the non-dimensional pressure as the model pressure increases, and the good agreement of the non-dimensional volumes of different scaled systems recommends this non-dimensional formalism, the GA optimization, and the numeric simulation of a surge transient, to design scaled experiments for modeling the IRIS pressurizer.

NOMENCLATURE

A =Flow area,
Fr =Froude number,
h =Enthalpy per unit mass,
k =Thermal conductivity,
K_p =Proportional constant of the PI controller
K_i = Integral constant of the PI controller
L =Length,
m =Mass,
$\dot{m}, W$ =Mass flow rate,
$N_0 = NW_{WC}$ = Mass flow wall condensation number
$N_1 = NW_{RO}$ = Rainout number,
$N_2 = N\dot{Q}_{WC}$ = Wall condensation heat number,
$N_3 = NW_{FL}$ = Flashing number,
$N_4 = \Psi$ = Pressure number,
$N_5 = NK$ = Integral pressure control number,
$N_6 = NK$ = Proportional pressure control number,
$N_7 = (NWh_{RO})_1$ = First enthalpy transport rainout number
$N_8 = (NWh_{RO})_2$ = Second enthalpy transport rainout number
$N_9 = (NWh_{FL})_1$ = First enthalpy transport flashing number
$N_{10} = (NWh_{FL})_2$ = Second enthalpy transport flashing number
$N_{11} = (NWh_{WC})_1$ = First enthalpy transport wall condensation number
$N_{12} = (NWh_{WC})_2$ = Second enthalpy transport wall condensation number
$N_{13} = (NWh_{WC})_3$ = Third enthalpy transport wall condensation number
$N_{14} = (NWh_{WC})_4$ = Forth enthalpy transport wall condensation number
p = Pressure,
$\dot{Q}$ = Thermal power,

S= Wall area,
T = Temperature,
t = Time,
u= Velocity,
V = Volume,
$v = x\frac{v_g}{\alpha} = \left(\frac{h - h_f}{h_{fg}}\right)\frac{v_g}{\alpha}$ = Volume per unit mass
$x = \frac{h - h_f}{h_{fg}}$ = Steam quality
$\alpha = x\frac{v_g}{v}$ = Vapor (void) fraction
γ_l = Bubble non-dimensional velocity,
ρ= Density,
μ= Viscosity,
σ= Surface tension

Subscripts: FL=Flashing, RO=Rainout, WC=Wall condensation, 0=Reference value PI=Proportional-integral, p=proportional, i=Integral, f=Saturated liquid g=Saturated vapor l=liquid volume, v=Vapor volume

REFERENCES

1. N. E. Todreas and M. S. Kazimi, *Nuclear Systems I – Thermal Hydraulic Fundamentals*, Taylor & Francis, Levittown, USA, (1993).
2. J. P. Holman, *Heat Transfer*, McGraw-Hill Book Company, Singapore (1989).
3. Whalley, P.B., *Two-Phase Flow and Heat Transfer*. Oxford University Press, New York, (1996).
4. J. F. Wilson, R. J. Grenda, and J. F. Patterson, "Steam Volume Fraction in a Bubbling Two-Phase Mixture," *Transactions of the American Nuclear Society*, **Vol. 4, section 37**, PP 356-357 (1961).
5. A. C. O. Barroso, B. D. Batista Fo., I. D. Arone, L. A. Macedo, P. A. B. Sampaio, and M. Morais, "IRIS Pressurizer Design," *Proceedings of the ICAPP*, Cordoba, Spain, Paper 3227 (2003).
6. J. N. Reyes, Jr. and L. Hochreiter, "Scaling analysis of the OSU AP600 test facility (APEX)**,"** *Nuclear Engineering and Design*, **Vol. 186**, pp. 53-109 (1998).
7. C. M. F. Lapa, P. A. de Sampaio, and C. M. N. A. Pereira, "A new approach to designing reduced scale thermal-hydraulic experiment**,"** *Nuclear Engineering and Design*, **Vol. 229**, No. 2/3, pp. 205-212 (2004).
8. A. C. O. Barroso and B. D. Batista Fo., "Refining the Design of the IRIS Pressurizer," Proceeding of the 5th International Conference on Nuclear Option in Countries with Small and Medium Electricity Grids, Dubrovnik, Croatia (2004).